Polarity- and molecular orbital-engineered host materials for stable and efficient blue thermally activated delayed fluorescence

Soo-Ghang Ihn (sg.ihn@samsung.com)
Samsung Advanced Institute of Technology https://orcid.org/0000-0003-1333-0546

Daun Jeong
Samsung Advanced Institute of Technology

Eunsuk Kwon
Samsung Advanced Institute of Technology

Sangmo Kim
Samsung Advanced Institute of Technology

Yeon Sook Chung
Samsung Electronics Co., Ltd.

Myungsun Sim
Samsung Advanced Institute of Technology

Jun Chwae
Samsung Advanced Institute of Technology

Yasushi Koishikawa
Samsung Advanced Institute of Technology

Soon Ok Jeon
Samsung Advanced Institute of Technology https://orcid.org/0000-0003-3188-1536

Jong Soo Kim
Samsung Advanced Institute of Technology

Joonghyuk Kim
Samsung Electronics Co., LTD

Sungho Nam
Samsung Advanced Institute of Technology

Hyeonho Choi
Samsung Electronics Co., Ltd. https://orcid.org/0000-0002-6884-8193

Sunghan Kim
Samsung Advanced Institute of Technology

Article

Keywords: thermally activated delayed fluorescence (TADF), host materials, molecular geometry, polarity, excited-state dipole

Posted Date: August 27th, 2020

DOI: https://doi.org/10.21203/rs.3.rs-61467/v1

Abstract

To utilize thermally activated delayed fluorescence (TADF) technology for future displays, it is necessary to develop host materials that can harness the full potential of blue TADF emitters. We suggest an elaborative approach for designing host molecules for blue TADF devices with simultaneously improved efficiency and stability. We significantly enhanced the delayed fluorescence quantum yield by engineering the molecular geometry, polarity, and excited-state dipole moment of host molecules based on 3',5-di(9H-carbazol-9-yl)-[1,1'-biphenyl]-3-carbonitrile. The engineerd hosts stabilized the charge-transfer excited states of TADF emitters, suppressed exciton quenching, and improved the charge balance in the emitting layer. Moreover, because the hosts are phosphine-oxide bond-free molecules, they are photochemically and electrochemically stable compared to bis[2-(diphenylphosphino)phenyl] ether oxide, the most popular high-polarity host. The devices employing the hosts exhibited a two-fold increase in external quantum efficiency and a 37-fold increase in operation lifetime compared to control devices with the same TADF emitter.

Introduction

In host–guest organic light-emitting diodes (OLEDs), the photophysical properties of the light-emitting molecules are strongly impacted by the host material,[1-4] Therefore, the host should be carefully considered to fulfill the intricate requirements of a given emitter. For example, to achieve high-performance OLEDs based on thermally activated delayed fluorescent (TADF) emitters, polarity of the host materialis particularly important owing to the strong charge transfer (CT) character of the excited states in TADF emitters. Host materials with high ground-state polarity are capable of stabilizing the CT excited states of TADF emitters due to electrostatic interactions between the excited-state dipole moment of the TADF emitter and the ground-state dipole momentof the host material.[5-7] A high-polarity hosts can reduce the lowest excited-state singlet energy (S_1) of the TADF emitter; therefore, the energy gap between S_1 and the lowest excited-state triplet energy (T_1) can be reduced. The emission peaks of the TADF emitters are thus shifted to longer wavelengths and their reverse intersystem crossing rate (k_{rISC}) and delayed fluorescence quantum yields (Φ_{DF}) are enhanced, which improves the maximum external quantum efficiency (EQE_{max}) of the TADF device.[8-11]

Bis[2-(diphenylphosphino)phenyl]ether oxide (DPEPO) exhibits high polarity, making it a popular host for blue TADF emitters with several studies demonstrating the outstanding EQE_{max} of DPEPO-based blue TADF device.[9-11] However, the band gap of DPEPO is too wide and its charge transporting ability is poor, which results in a high driving voltage, poor electrochemical stability, and relatively short device operation lifetime. Moreover, DPEPO has photochemically unstable phosphine–oxide (P–O) bonds which induce faster degradation.[12-14] Hence, no studies have reported long operation lifetimes of DPEPO-based TADF devices. On the other hand, several highly stable blue TADF devices have been obtained with stable hosts such as 3,3’-di(9H-carbazol-9-yl)-1,1’-biphenyl (mCBP) and 3',5-di(9H-carbazol-9-yl)-[1,1'-biphenyl]-3-carbonitrile (mCBP-CN), yet at the expense of efficiency.[14-16]

Herein, we introduce alternative host materials that are capable of stabilizing the CT excited-states of TADF emitters owing to their relatively high ground-state polarity, while simultaneously providing long OLED operation lifetimes owing to their narrower band gaps, better charge transporting ability, and greater material stability compared to P–O bond-based DPEPO. The novel host material-based blue TADF devices exhibit similar performance to those using DPEPO, and are as stable as those using mCBP-CN. The simultaneous achievement of high efficiency and stability of these high-polarity and P–O bond-free compounds makes them suitable alternative host materials for DPEPO- and mCBP-CN.

Results

Molecular asymmetry and polar groups introduce high polarity to P-O bond-free host materials

The ability to stabilize the CT excited state of TADF emitters primarily depends on the geometry and electrostatic properties of the host materials. The dipole moment can serves as a convenient polarity scale because of its dominant contribution to the electrostatic interactions between the emitter and host molecules. With the aim of designing a P–O bond-free host with high polarity, we introduced asymmetry and polar groups into the molecular geometry of a leading molecule to control the dipole moment. As a leading molecule, we considered mCBP-CN (Figure 1), an electron-transporting host derivatized from mCBP by attaching a polar cyano (CN) group to one of the two phenyls. The asymmetrically attached CN group increased the ground-state dipole moment, μ_{GS}, to 3.4 D (debye, where 1 D $\approx$ 3.34 x 10^{-30} C·m). However, its μ_{GS} still much lower than that of DPEPO.

By modifying the asymmetry and polar groups of mCBP-CN, we obtained four novel host materials, H1–H4, with improved μ_{GS} values (Figure 2a, first panel). H1 was obtained by modifying the bond position of one of the carbazole groups of mCBP-CN from meta to ortho to induce asymmetry,t hereby increasing μ_{GS} to 4.18 D. H2 was obtained by attaching two additional CN groups to the second carbazole group of H1, which induced a much higher μ_{GS} of 6.84 D. H3 was achieved by substituting the second carbazole group of H1 with a benzofuran group; the introduction of a heteroatom, oxygen, slightly improved the μ_{GS} value (4.63 D) over that of H1. Finally, an additional CN-functionalization on the dibenzofuran group of H2 resulted in H4, which exhibited a much higher μ_{GS} of 7.64 D. Notably, the μ_{GS} values of H2 and H4 are close to the value of 8.05 D for DPEPO.

To experimentally compare the ground-state polarities of the host materials, we measured their retention times with high-performance liquid chromatography (HPLC). The elution order of solutes in HPLC is governed by polarity.[17] Therefore, HPLC measurements provide details about the polarity of materials. H1–H4 and DPEPO showed shorter HPLC-retention times than mCBP and mCBP-CN (Figure 2a, second panel), indicating that H1–H4 and DPEPO have higher ground-state polarities. DPEPO had the shortest HPLC-retention time, suggesting that it is still the most powerful host for enhancing TADF efficiency. Consequently, the HPLC-retention times can scale the examined host materials as well as the ground-

state dipole moments does but they have an inverse tendency. Figure 2b shows the correlation between them. The correlation coefficient, R^2 is −0.75 when considering DPEPO and −0.88 without DPEPO.

To explore their suitability as host materials for TADF emitter molecules, we investigated whether the excited-state energies (S_1 and T_1) of H1–H4 would be high enough to confine excitons within a given blue TADF emitter, 1PCTrz which has a typical structure of twisted intramolecular charge transfer (TICT) molecules (Figure 2c).[18] Our calculations indicated that H1–H4 had sufficiently higher S_1 and T_1 values (Figure 2a, third panel) than the given TADF emitter. To verify the ground-state polarities of the host materials and investigate their effect on the photophysical properties of the TADF emitter, we compared photoluminescence (PL) spectra of thin films composed of the given TADF emitter and host material.

According to the work of Lippert *et al.*,[19] polar solvents can redshift the emission of TICT molecules which are popular TADF emitters. In addition, the polarity of the solvents changes the emission state of TICT molecules between a locally excited (LE) state and CT state by changing the twist angle between the electron accepting moiety (A) and electron donating one (D).[20] When fabricated with H1–H4 and DPEPO, 1PCTrz exhibited redshifted and broadened PL emission compared to that with mCBP and mCBP-CN, as shown in Figure 2d. The PL peak wavelengths and full-width at half maximum (FWHM) values for all the tested host:1PCTrz (host:1PCTrz) films are summarized in Table 1.

High polarity hosts enhance the reverse intersystem crossing rate and delayed fluorescence quantum yield

The primary purpose of employing high-polarity hosts for TADF devices is to deduce their potential for stabilizing the CT excited states of TADF emitters, in the manner of DPEPO. The improved EQE_{max} of DPEPO-based TADF devices originates from the enhanced reverse intersystem crossing rate, k_{rISC}, and delayed fluorescence quantum yield, Φ_{DF}, of the TADF molecules owing to the high-polarity DPEPO matrix. Such enhancements are the origin of the improved EQE_{max} of TADF devices employing DPEPO as a host. Based on the results of PL experiments in Figure 2d, we expected H1–H4 to have the same effect as DPEPO.

The k_{rISC} values were calculated using the equations presented by Zeng et al.[21] Table 1 shows that 1PCTrz exhibited higher Φ_{DF} and k_{rISC} values when hosted in H1–H4 than in mCBP and mCBP-CN. This is ascribed to the high polarity of H1–H4, as indicated by the enhanced μ_{GS} values. However, Φ_{DF} did not monotonically increase with μ_{GS}, even when comparing hosts with the same core structure. H2 and H4, which have μ_{GS} values near 7 D exhibited lower Φ_{DF} values than H1 and H3. It should be noted that the dipole moment of the host has two sides in relation with Φ_{DF}. In the ground state, a high dipole moment enhances delayed fluorescence; while in the excited state, it facilitates exciton quenching through intermolecular CT owing to interactions with the emitter dipoles in the CT excited state.[7] The excited-state dipole moments (μ_{ES}) are given in Figure 2a and Table 1. H2 and H4, which have high μ_{GS} values, exhibit higher μ_{ES} values and relatively low Φ_{DF} values. This implies that their CT-character is strengthened in the

excited state, and thereby enhancing exciton quenching. The formation of intermolecular CT complexes depends on the energy-level structures of the host and emitter molecules. Although μ_{ES} value of DPEPO is slightly below that of H2 (11.06 vs. 11.73 D), its Φ_{DF} value is higher (46.5% vs. 37.9%). This is because the extremely wide bandgap of DPEPO suppresses the formation of intermolecular CT complexes.

The effect of these excited-state dipole moments on the performance of TADF devices is discussed later. Considering the higher Φ_{DF} and k_{rISC} values and redshifted and broadened emission of 1PCTrz in the novel high-dipole moment host materials (H1–H4), we expect them to be strong candidates for replacing both high-polarity hosts such as DPEPO and stable hosts such as mCBP-CN.

Ground-state characteristics of the high-dipole moment host materials

Although donor–acceptor (D–A) type TADF emitters have bipolar characteristics, they largely show hole-transporting behavior when used with electron-transporting host materials such as mCBP-CN.[14] TADF devices typically have high emitter/host compositional ratios compared to other technologies such as a fluorescent and phosphorescent OLEDs; therefore, to provide high efficiency and stability, an electron transporting-host such as mCBP-CN is required, which forms a mixed-host-like emitting layers with hole-transporting TADF emitters. In this work, the employed TADF emitter, 1PCTrz, exhibits hole-transporting behavior rather than electron-transporting behavior, although it is basically a bipolar D–A molecule as shown in Figure 3. Thus, the host should exhibit electron-transporting properties.

The designed hosts, H1–H4, all exhibit electron-transporting behavior (Figure 3). According to our calculations, H1–H4 have comparable LUMOs to that of 1PCTrz, yet much lower highest occupied molecular orbitals (HOMOs) than both 1IPCTrz and mCBP, in a similar manner to mCBP-CN. Our previous work[14] revealed that electron-transporting hosts can form mixed-host-like emitting layers with highly doped TADF emitters, which can improve the stability of TADF devices. Note that H1 and H2, which have the same core structure show different HOMO and LUMO energy levels. Specifically, H2 has lower-lying HOMO and LUMO energy levels than H1, which indicates that H2 has stronger electron-transporting behavior. H4 also has stronger electron transport than than H3. It is interesting to compare H2 with H1 and H4 with H3, particularly from view point of stability, whch we will discuss in the following section.

Device performances

The device characteristics of the tested OLEDs are shown in Figure 4and their performances are summarized in Table 2. The OLEDs were fabricated with the following layer stacks: indium tin oxide (ITO)/p-doped (3 wt%, NDP series, see the Device fabrication and measurement section) N-([1,10-biphenyl]-4-yl)-9,9-dimethyl-N-(4-(9-phenyl-9H-carbazol-3-yl) phenyl)-9H-fluoren-2-amine (BCFA) (10 nm)/BCFA (135 nm)/2,2'-di(9H-carbazol-9-yl)-1,1'-biphenyl (oCBP) (10 nm)/host:1PCTrz (40 nm)/2,8-bis(diphenylphosphine oxide) dibenzofuran (DBFPO) (10 nm)/co-deposited NET:NDN series (5:5 by volume, 30 nm, see the Device fabrication and measurement section)/Al. The device structure is the same as the OLED device reported by Hong, S. *et al.*,[22] except for the emitting layer and electron transport layer.

The normalized electroluminescence (EL) spectra (Figure 4a) of the TADF devices look similar to the nomalized PL spectra (Figure 2d), with only small differences ascribed to weak micro-cavity effects in multilayered OLEDs.[23] Thus, in the same manner as the PL spectra, the electroluminescence spectra of the TADF devices employing high-polarity hosts (H1–H4, DPEPO) were slightly redshifted and broader than those of the OLEDs based on mCBP or mCBP-CN. This result indicates that host polarity has the same effect in the electrically driven multilayered OLEDs as in the optically pumped single-layer thin films.

Figure 4b shows the current density–voltage characteristics of the OLEDs. The DPEPO-based OLED, which has the widest bandgap (5.43 eV, calculated) showed the highest device resistance; while mCBP-CN has the second narrowest bandgap (3.73 eV, Figure 3) shows the smallest device resistance. Although H1 has the narrowest bandgap (3.71 eV, Figure 3), the device resistance of H1 is higher than that of mCBP-CN, because the difference in device resistance is very small, yet mCBP-CN has a lower LUMO, which may facilitate charge transport within the highly doped hole-transporting TADF emitter.[14]

Figure 4c shows the EQE–luminance characteristics of the OLEDs. The devices employing H1–H4 exhibit higher $EQE_{max}$of 13.6%–18.0% than the mCBP-based (10.0%) and mCBP-CN-based (9.1%) OLEDs. These high EQE_{max} values can be attributed to the increased delayed fluorescence of 1PCTrz in H1–H4, as these hosts provide highly a polar environment. The H3:1PCTrz film exhibits the highest Φ_{DF} among the 1PCTrz-doped films employing P–O bond-free hosts (H1–H4, mCBP, and mCBP-CN) and consequently the H3:1PCTrz-based OLED exhibits the highest EQE_{max}. Notably, the EQE_{max} of the H3:1PCTrz-based OLED is the closest to that of the DPEPO:1PCTrz-based OLED (18.0% vs. 21.1%). Furthermore, at practical brightnesses (500 or 1,000cd m^{-2}, for example), the EQE of the H3:1PCTrz-based OLED exceeds that of the DPEPO:1PCTrz-based OLED as efficiency roll-off is suppressed in the former. Despite the short delayed fluorescence lifetime (τ_{DF}) of the DPEPO system, DPEPO:1PCTrz-based OLEDs exhibit significant efficiency roll-off owing to the inferior property of DPEPO.[14] Although τ_{DF} for the H1–H4 systems were longer than those for the DPEPO system, the devices based on H1–H4 showed higher EQEs at a high luminance (1,000 cd m^{-2}). This is attributed to the improved charge balance in the emitting layer, where a lower LUMO level of H1–H4 leads to increased injection of electrons.

It is noteworthy that the EQE_{max} values for the devices based on H1–H4 varied consistently with Φ_{DF}, indicating that the effects of host polarity observed in the optical experiments are also applicable to the electrical devices. Among H1–H4, H3 exhibits the highest EQE_{max}, despite its relatively low μ_{GS} (4.63 D, Table 1). This can be explained by its low μ_{ES} (5.04 D). We believe that excitons from the 1PCTrz can be significantly quenched by hosts (H2 and H4) as their excited-state polarities are much higher than that of H3, inducing easier formation of intermolecular CT complexes. In contrast, in H3, 1PCTrz can avoid serious exciton quenching in H3 owing to the low μ_{ES} of H3 and small μ_{ES} gap (1.84 D) between H3 and 1PCTrz, with affects the influence of the excited-state dipole field of the host.[7] Nevertheless, the DPEPO-based OLED still has the greatest EQE_{max} (21.1%), despite DPEPO having the highest μ_{ES} (11.06D). This

is because the extremely wide band gap of DPEPO makes it difficult for it to reach the excited state or form an intermolecular CT complexes with other molecules. Although the μ_{ES} of H1 is lower than that of H3 (3.8 vs. 5.04 D), its EQE_{max} is only very slightly lower (17.9% vs. 78.0%) owing to its lower μ_{GS} (4.18 vs. 4.63 D). From the perspective of effciency, H1 and H3 are probably the most promising candidates as alternative hosts for blue TADF devices.

To investigate the influence of the host materials on the device stability, the operation lifetimes of OLEDs with different host materials were measured at an initial luminance of 500 cd m^{-2}. The decreases in luminance with increasing OLED operation time was measured using the LT50 parameter, which represents the time at which the luminance decreased to 50% of the initial luminance. Figure 4d shows the normalized luminance of the OLEDs as a function of OLED operation time under a constant current density at the initial luminance of 500 cd m^{-2}. Consistently with the previous report in which mCBP-CN was suggested as a stable host,[14] the LT50 of the OLED fabricated using mCBP-CN (36.2 h) was much longer than that of the DPEPO-based OLED (0.6 h) and the conventional mCBP-based OLED (3.3 h). Nevertheless, the H2-, H3- and H4-based OLEDs notably exhibit much longer operational lifetimes than not only the DPEPO- and mCBP-based OLEDs, but also the mCBP-CN-based OLED. In particular, the H3-based OLED exhibited an operational lifetime comparable to that of the stable mCBP-CN-based OLED, while simultaneously exhibiting remarkably improved efficiency (Figure 4c). Furthermore, the H2- and H4-based OLEDs exhibited much longer LT50 (122.4 and 86.9 h, respectively) than even the mCBP-CN-based OLED. While the mCBP-CN-based OLED had the best charge transport characteristics as shown in Figure 4b, and the most suppressed efficiency roll-off, as shown in Figure 4c, indicating the best charge balancing ability, its EQE at a practical brightness and LT50 were inferior to those of the OLEDs based on H2–H4.

As we discussed with Figure 1, the simulataneously high efficiency and OLED operational stability are attributed to the high polarity of the novel hosts, stabilizing CT excited states of 1PCTrz, and the P–O bond-free molecular structure with strong electron-transporting character, which enhances operational stability. However, the LT50 of the H1-based OLED was shorter than that of the mCBP-CN-based OLED (21.7 vs. 36.2 h), while its EQE was superior. This exception can be explained by considering the charge transporting character of H1. Owing to the CN-functionalization, the four novel host materials (H1–H4) all have low-lying HOMO and LUMO levels (Figure 1b), which provides electron-transporting characteristics and high device stability with highly doped (20vol% here) hole-transpoting TADF emitters.[14] With this knowledge, the shorter LT50 of the H1-based OLED can be explained by considering the shallower LUMO energy level of H1, which indicates weaker electron-transporting character. This explanation is valuable when compariing the device operation lifetimes of the OLEDs based on the high-polarity host materials with the same core strucutres (H1 and H2; H3 and H4). The H2-based TADF device exhibits a much longer device operation lifetime than the H1-based device (1224.4 vs. 21.7 h), probably because H2 has a lower LUMO than H1 (–2.04 vs. –1.75 eV). Meanwhile, the H4-based TADF device exhibits a longer device operation lifetime than H3-based device (86.9 vs. 55.1 h) for the same reason; the LUMO energy levels of H4 and H3 are–1.79 eV and–1.64 eV, respectively. Through those comparisons, we can conclude that

host materials with lower lying LUMO are more suitable for enhancing device stability of TADF devices that employ highly doped hole-transporting TADF emitters.

Characteristics and stability of hole-only devices (HODs) and electron-only devices (EODs)

To investigate the material stability of the novel hosts and explain the longer operational lifetimes of their OLEDs, we performed charge transport stability test of the host films in hole-only devices (HODs) and electron-only devices (EODs). Figure 5a and b show the current density–voltage(*J*– *V*) characteristics of the HODs and EODs, respectively. The EODs with the high-polarity hosts had much lower turn-on voltages than the HODs, indicating that they are electron-transporting hosts, similarly to mCBP-CN. Electron-transporting hosts are well-suited touse with hole-transporting TADF emitters with a shallow HOMO and high doping concentration, which facilitates the fabrication of stable OLEDs.[14] Figure 5cand d show the increment of the driving voltages (V_d) of the HODs and EODs, respectively, under the same current density (50 mA cm^{-2}) as a function of time. The increase of V_d is equivalent to the increase of resistivity induced by material degradation.[24] For all the novel high-polarity hosts (H1–H4), the HODs and EODs showed much smaller increments in V_d during operation than DPEPO-based HOD and EOD. This indicates that the novel high-polarity hosts will degrade much slower than DPEPO under the same electrical stress, in the same manner as mCBP-CN.

Photoluminescence stability

To investigate and compare the excited-state stabilities of the hosts, we performed a PL-stability study by exposing the films to a UV laser for 3h. Figure 6a and b show normalized PL spectra of 50-nm H2 and mCBP films, respectively, in the as-deposited and degraded (3-h UV-laser-exposed). Normalization was performed by dividing the spectra by the PL peak intensity of the as-deposited film. The peak intensity for the H2 film decreased to 76% of its initial value after 3-h exposure to UV-laser, while that of mCBP decreased to 36%. This significant difference in PL stability correlates with the great difference in device operation lifetime between the H2- and mCBP-based OLEDs (LT50 = 122.4 and 3.3h, respectively, Table 2). The other high-polarity hosts also exhibited high PLstability (Supplementary Figure 2), as did mCBP-CN in the previous report.[14] We were unable to perform PL stability studies on DPEPO because it requires a higher energy laser for excitation. However, a few articles have reported low photochemical stability of the P–O bond,[12,13] and we have previously discussed the poor PL stability of DPEPO and its substitutions with two P–O bonds.[14]

We performed further PL stability studies with 1PCTrz-doped host films, which enables the excited-state stability to be investigated without detrimental host interactions such as concentration quenching, triplet-triplet annihilation, exciton migration, etc.[25-29] Figure 6c, d and e show normalized PL spectra of 50-nm H2:1PCTrz, mCBP:1PCTrz and DPEPO:1PCTrz films, respectively. The peak intensity for the H2:1PCTrz film decreased to 80% of its initial value after 30h UV-laser exposure, while that for the mCBP:1PCTrz and DPEPO:1PCTrz films decreased to71% and 68%, respectively. This result also explains the longer operational lifetime of the H2:1PCTrz-based OLEDs, although the decrement of the peak intensity for

mCBP:1PCTrz and DPEPO:1PCTrz films was reduced when compared to that for the host-only films. The improved PL stability after 1PCTrz doping is attributed to the host-to-guest energy transfer for mCBP. However, for DPEPO, the unexpectedly low loss of intensity after 1PCTrz doping is related to the fact that DPEPO was not excited during the DPEPO:1PCTrz film PL measurement, so it did not suffer the degradation induced by the weak P–O bond. The other emitting layer films (H1:1PCTrz, H3:1PCTrz, and H4:1PCTrz) also exhibited higher PL stabilities than the mCBP:1PCTrz and DPEPO:1PCTrz films. Their normalized PL spectra before and after 3-h UV-laser exposure are presented in Supplementary Figure S2.

Orientation of transition dipole moments

To further verify the mechanism of host polarity-induced efficiency enhancement, we performed angle-dependent PL measurements with various host films doped with 1PCTrz, which enables the cause of the improved EQE_{max} to be more closely examined. In particular, we can observe if it originates from light out-coupling effects instead of host polarity. Figure 7a shows the angle-dependent PL spectrum of *p*-polarized light from the 50-nm-thick 1PCTrz-doped H2 host film, while the angle-dependent PL intensities for H2:1PCTrz are depicted in Figure 7b (magenta squares). A theoretical fit of the data reveals a horizontal orientation of the transition dipole moments ($h/(h+v)$) of 0.89. This value is quite far from the value for an isotropic orientation ($h/(h+v) = 0.67$), which indicates that the orientation effect is significant. However, the mCBP-CN:1PCTrz film also exhibits a comparable $h/(h+v)$ value of 0.88. This means that the significant difference in EQE_{max} between the H2- and mCBP-CN-based OLEDs is not attributed to orientation effects. Moreover, in spite of the small $h/(h+v)$ of 0.79 of the H3:1PCTrz emitting layer, which indicates low out-coupling efficiency, the OLED with the H3:1PCTrz emitting layer exhibited the highest EQE_{max} among the OLEDs with P–O bond-free hosts. For the tested films, there were no significant differences in the $h/(h+v)$ values, with the exception of the H3:1PCTrz film. This indicates that the enhanced EQE_{max} observed with high-polarity host-based TADF OLEDs is not attributed to the orientation effect. Considering the results of the PL spectrospcopic study, including the redshifted and broadened emission peaks and higher delayed fluorescence quantum yields with high-polarity host-based films, we conclude that the enhanced efficiencies of the TADF devices are ascribed to the stabilization of the CT excited states of the TADF emitter when surrounded by high-polarity host molecules. The values of $h/(h+v)$ for all the tested films are summarized in Table 3 along with their expected out-coupling efficiencies. The angle-dependent PL intensities for the other hosts and their theoretical fit are presented in the Supplementary Figure 3).

Discussion

We designed, synthesized and verified four new P–O bond-free host materials, H1–H4, for use with a blue TADF emitter molecule, 1PCTrz. The host materials had molecular asymmetry and large electric dipole moments. The TADF devices based on the novel hosts exhibited high efficiencies approaching that of the DPEPO-based TADF device. At the same time, they achieved much longer operational lifetimes than those based on DPEPO, mCBP and mCBP-CN. This simultaneous improvement in efficiency and stability is attributed to the intricate properties of the host materials that works consonantly toward enhanced device

operation: i) high polarity stabilizes the CT excited state of the TADF emitter; ii) a relatively low excited-state dipole moment suppresses intermolecular CT-induced quenching of excitons; iii) electron-transporting character allows hole transport/electron transport mixed-host-like behavior in the emitting layer owing to the hole-transporting ability of the highly doped TADF emitter; and iv) P–O bond-free design improves photochemical stability. The novel hosts adopt asymmetric molecular structures and polar groups appropriately to provide a trade-off between high ground-state dipole moments and low excited-state dipole moments, while simultaneously modulating their molecular orbital energy levels. Our strategy for designing hosts with particular characteristics will promote the commercialization and success of TADF devices and technology.

Methods

Calculations of dipole moment. The molecular structures of the P–O bond-free hosts considered in this study have rotatable bonds and thus allow various conformations, which might give a wide range of dipole moments. We estimated that the dipole moment may affect the polarity of the host matrix. In order to find an appropriate set of conformers, we used a conformational search module included in Schrödinger software[30] that collects structures using the mixed torsional/low-mode sampling method starting from a given structure. A set of representative conformers were determined from the local minimization starting from numerous structures. In the minimization, the energies were evaluated in the classical level using the OPLS3e force field. For all conformers, we performed optimizations through density functional theory (DFT) calculations at the level of B3LYP/6-31G(d) and obtained the values of dipole moments using Jaguar software.[31] We determined the representative value of dipole moment, denoted by μ_{GS}, to be the one calculated from the structure with the minimum energy among the conformers. The minimum and the maximum values of the dipole moments in company with μ_{GS} for all hosts are displayed in Supplementary Fig. 1. The P–O bond-free hosts exhibited a considerable variation of dipole moments according to conformations. We regarded μ_{GS} as a polarity scale for convenience in this study; however, one may consider the range of dipole moments due to the conformer distribution of the host, where the hosts may have similar μ_{GS} but distinguished polarities.

General Procedures of synthesis and characterization. Chemicals were purchased from Sigma-Aldrich Co., Tokyo Chemical Industry Co., 4chem Laboratory Co., Ltd., Medigen Co. Ltd., and Hanchem Co., Ltd. and used without further purification. ^{1}HNMR and ^{13}CNMR spectra were recorded on a Bruker ASCEND 500 at 500 MHz using CD_2Cl_2 as the solvent. The ion trap time-of-flight liquid chromatograph mass spectrometer (LCMS-IT-TOF) system instrument consisted of LC-30A Nexera SR system instrument (Shimadzu) connected to a hybrid IT-TOF mass spectrometer equipped with an electrospray ionization source (Shimadzu).

Synthesis of H1. A mixture of 3-bromo-2-(9*H*-carbazol-9-yl)benzonitrile (**1**) (6.81 g, 19.62 mmol), 9-(3-(4,4,5,5-tetramethyl-1,3,2-dioxaborolan-2-yl)phenyl)-9*H*-carbazole (**5**) (15.12 g, 39.25 mmol), potassium carbonate (5.42 g, 39.25 mmol), and tetrakis(triphenylphosphine)palladium(**0**) (2.27 g, 1.96 mmol) in

70 mL of THF/water (2.5:1) was stirred at 85 °C for 12 h. After allowing it to cool to room temperature, the reaction mixture was diluted with methanol and filtered. The resulting solid was purified by column chromatography using dichloromethane/*n*-hexane (1:2) as eluent. The white solid obtained after evaporating the solvent was recrystallized from ethyl acetate and finally dried under vacuum to give *2,3'-di(9H-carbazol-9-yl)-[1,1'-biphenyl]-3-carbonitrile* (**H1**) (5.40 g, 54%). The synthetic routes for the hosts are displayed in Supplementary Fig. 4. **^{1}H NMR** (500 MHz, CD_2Cl_2): δ 8.13 (d, J = 7.7 Hz, 2H), 8.06 (dd, J = 7.7, 0.4 Hz, 2H), 7.96 (d, J = 7.7 Hz, 2H), 7.78 (t, J = 7.8 Hz, 1H), 7.38 (t, J = 8.0 Hz, 2H), 7.21–7.31 (m, 9H overlap), 7.08 (d, J = 8.2 Hz, 2H), 7.09 (d, J = 2.7 Hz, 1H), 6.79 (d, J = 8.2 Hz, 2H); **^{13}C NMR** (126 MHz, CD_2Cl_2): δ 143.23, 141.3, 141.2, 139.4, 138.2, 138.0, 136.7, 134.5, 130.4, 130.3, 127.6, 124.2, 126.8, 126.4, 124.1, 123.6, 121.2, 121.2, 120.6, 120.4, 116.4, 115.5, 110.3, 109.9; **LCMS-IT-TOF**: 510.19 [$(M + H)^+$]. See Supplementary Figs. 5 and 6.

Synthesis of H2. A mixture of 3'-bromo-2-(9*H*-carbazol-9-yl)-[1,1'-biphenyl]-3-carbonitrile (**3**) (5.48 g, 12.06 mmol), 9*H*-carbazole-3,6-dicarbonitrile (3.93 g, 18.09 mmol), potassium carbonate (5.00 g, 36.19 mmol), 1,10-phenanthroline (4.35 g, 24.12 mmol), and copper iodide (2.30 g, 12.06 mmol) in 30 mL of dimethylacetamide was stirred at 170 °C for 15 h. After allowing it to cool to room temperature, the reaction mixture was diluted with methanol, filtered, and dried. The resulting solid was diluted with DMF and filtered with silica gel. The yellow solid obtained after evaporating the solvent was recrystallized from 1,4-dioxane and finally dried under vacuum to give 9-(2'-(9*H*-carbazol-9-yl)-3'-cyano-[1,1'-biphenyl]-3-yl)-9*H*-carbazole-3,6-dicarbonitrile (**H2**) (5.40 g, 47%). **^{1}H NMR** (500 MHz, CD_2Cl_2): δ 8.38 (d, J = 1.1 Hz, 2H), 8.08 (d, J = 7.7 Hz, 2H), 7.99 (td, J = 7.7, 1.5 Hz, 2H), 7.81 (t, J = 7.8 Hz, 2H), 7.59 (dd, J = 8.6, 1.5 Hz, 2H), 7.31–7.37 (m, 4H overlap), 7.17 (dt, J = 6.2, 1.7 Hz, 1H), 7.01–7.04 (m, 3H overlap), 6.65 (d, J = 7.6 Hz, 2H); **^{13}C NMR** (126 MHz, CD_2Cl_2): δ 143.6, 142.6, 141.2, 139.9, 137.9, 136.5, 135.7, 134.9, 131.1, 130.9, 130.5, 129.6, 127.7, 127.0, 126.9, 126.0, 124.0, 122.7, 121.3, 121.1, 121.1, 120.1, 116.2, 115.7, 111.4, 110.2, 104.7; **LCMS-IT-TOF**: 560.17 [$(M + H)^+$]. See Supplementary Figs. 7 and 8.

Synthesis of H3. 2-(9*H*-Carbazol-9-yl)-3-(dibenzo[*b*,*d*]furan-2-yl)benzonitrile (**H3**) was obtained as white crystal (13.50 g, 66%) from 3-bromo-2-(9*H*-carbazol-9-yl)benzonitrile (**1**) (16.38 g, 47.18 mmol) and dibenzo[*b*,*d*]furan-2-ylboronic acid (10.00 g, 47.18 mmol) using a procedure analogous to that used for 2,3'-di(9*H*-carbazol-9-yl)-[1,1'-biphenyl]-3-carbonitrile (**H1**). **^{1}H NMR** (500 MHz, CD2Cl2): δ 8.04 (d, J = 7.8 Hz, 2H), 8.01 (dd, J = 7.9, 1.5 Hz, 2H), 7.96 (dd, J = 7.8, 1.5 Hz, 2H), 7.79 (t, J = 7.8 Hz, 1H), 7.59 (d, J = 1.9 Hz, 1H), 7.55 (d, J = 7.7 Hz, 1H), 7.45 (d, J = 8.2 Hz, 1H), 7.40 (td, J = 7.2, 1.2 Hz, 1H), 7.35 (td, J = 7.2, 1.1 Hz, 2H), 7.21–7.28 (m, 3H overlap), 7.15 (d, J = 8.6 Hz, 1H), 7.04–7.09 (m, 3H overlap); **^{13}C NMR** (126 MHz, CD2Cl2): δ 156.9, 156.3, 144.1, 141.4, 137.9,136.9, 133.9, 130.3, 128.0, 127.3, 126.7, 124.7, 124.1, 123.9, 123.4, 121.0, 120.9, 120.6, 116.6, 115.7, 112.1, 111.8, 110.2; **LCMS-IT-TOF**: 435.16 [(M + H)+]. See Supplementary Figs. 9 and 10.

Synthesis of H4. 8-(2-(9*H*-Carbazol-9-yl)-3-cyanophenyl)dibenzo[*b*,*d*]furan-2-carbonitrile (**H4**) was obtained as white crystal (4.50 g, 45%) from 2-(9*H*-carbazol-9-yl)-3-(4,4,5,5-tetramethyl-1,3,2-dioxaborolan-2-yl)benzonitrile(**2**) (12.87 g, 32.64 mmol) and 8-bromodibenzo[*b*,*d*]furan-2-carbonitrile (5.92 g,

21.76 mmol) using a procedure analogous to that used for 2,3'-di(9*H*-carbazol-9-yl)-[1,1'-biphenyl]-3-carbonitrile (**H1**). **^{1}H NMR** (500 MHz, CD_2Cl_2): δ 8.03 (d, J = 7.8 Hz, 2H), 7.99–8.01 (m, 2H overlap), 7.86 (d, J = 1.4 Hz, 1H), 7.82 (t, J = 7.8 Hz, 1H), 7.68 (dd, J = 8.5, 1.6 Hz, 1H), 7.62 (d, J = 1.6 Hz, 1H), 7.53 (d, J = 8.5 Hz, 1H), 7.35 (td, J = 7.3, 1.2 Hz, 2H), 7.23 (t, J = 7.5 Hz, 2H), 7.20 (d, J = 8.6 Hz, 1H), 7.13 (dd, J = 8.6, 6.8 Hz, 1H), 7.07 (d, J = 8.0 HZ, 2H); **^{13}C NMR** (126 MHz, CD_2Cl_2): δ 158.7, 156.8, 143.5, 141.4, 138.01, 136.8, 134.2, 133.2, 131.8, 130.5, 128.9, 126.8, 125.7, 125.1, 123.9, 123.2, 121.1, 121.0, 119.4, 116.5, 115.8, 113.4, 112.3, 110.1, 107.4; **LCMS-IT-TOF**: 460.14 [$(M + H)^+$]. See Supplementary Figs. 11 and 12.

Synthesis of Precursor 1. A solution of 9*H*-carbazole (36.12 g, 216.00 mmol) in anhydrous N,N-dimethylformamide (DMF) was added dropwise into dispersion of sodium hydride (60%, 8.64 g, 216.00 mmol) in anhydrous DMF in an ice bath. After stirring for 1 h, 3-bromo-2-fluorobenzonitrile (47.52 g, 237.60 mmol) was dissolved in anhydrous DMF and added to the stirred reaction mixture under a nitrogen atmosphere. The reaction mixture was stirred at 130 °C for 15 h. After allowing it to cool to room temperature, the reaction mixture was extracted with dichloromethane and water. The organic layer was dried using magnesium sulfate and evaporated with a rotary evaporator. The crude product was purified by column chromatography using dichloromethane/*n*-hexane (1:2) and then dried under vacuum to give 3-bromo-2-(9*H*-carbazol-9-yl)benzonitrile (**1**) (51.50 g, 69%). See Supplementary Fig. 2.

Synthesis of Precursor 2. A mixture of 3-bromo-2-(9*H*-carbazol-9-yl)benzonitrile (**1**) (34.35 g, 98.91 mmol), bis(pinacolato)diboron (37.68 g, 148.37 mmol), potassium acetate (29.12 g, 296.74 mmol), and [1,1'-bis(diphenylphosphino)ferrocene]dichloropalladium(II) (7.24 g, 9.89 mmol) in 250 mL of anhydrous DMF was stirred at 150 °C for 12 h. After allowing it to cool to room temperature, the reaction mixture was extracted with dichloromethane and water. The organic layer was dried using magnesium sulfate and evaporated with a rotary evaporator. The crude product was purified by column chromatography using dichloromethane/*n*-hexane (1:1) and then dried under vacuum to give 2-(9*H*-carbazol-9-yl)-3-(4,4,5,5-tetramethyl-1,3,2-dioxaborolan-2-yl)benzonitrile(**2**) (25.10 g, 64%).

Synthesis of Precursor 3. A mixture of 2-(9*H*-carbazol-9-yl)-3-(4,4,5,5-tetramethyl-1,3,2-dioxaborolan-2-yl)benzonitrile (**2**) (10.02 g, 25.42 mmol), 1-bromo-3-iodobenzene (10.79 g, 38.14 mmol), tripotassium phosphate (16.19 g, 76.27 mmol), SPhos (1.04 g, 2.54 mmol), and bis(dibenzylideneacetone)palladium(**0**) (0.73 g, 1.27 mmol) in 64 mL of toluene/water (10:1) was stirred at 100 °C for 13 h. The reaction mixture was extracted with toluene and water. The organic layer was dried using magnesium sulfate and evaporated with a rotary evaporator. The crude product was purified by column chromatography using dichloromethane/n-hexane (1:1) and then dried under vacuum to give 3'-bromo-2-(9*H*-carbazol-9-yl)-[1,1'-biphenyl]-3-carbonitrile (**3**) (5.00 g, 45%).

Synthesis of Precursor 4. A mixture of carbazole (12.97 g, 77.59 mmol), 1-bromo-3-fluorobenzene (20.37 g, 116.38 mmol), and cesium carbonate (50.56 g, 155.18 mmol) in 190 mL of dimethylacetamide was stirred at 160 °C for 12 h. After allowing it to cool to room temperature, the reaction mixture was extracted with dichloromethane and water. The organic layer was dried using magnesium sulfate and evaporated with a rotary evaporator. The crude product was purified by column chromatography using

dichloromethane/*n*-hexane (1:5) and then dried under vacuum to give 9-(3-bromophenyl)-9*H*-carbazole(**4**) (22.00 g, 88%).

Synthesis of Precursor 5. 9-(3-(4,4,5,5-Tetramethyl-1,3,2-dioxaborolan-2-yl)phenyl)-9*H*-carbazole (**5**) was obtained as white crystal (16.10 g, 81%) from 9-(3-bromophenyl)-9*H*-carbazole (**4**) (17.45 g, 54.16 mmol) using a procedure analogous to that used for 2-(9*H*-carbazol-9-yl)-3-(4,4,5,5-tetramethyl-1,3,2-dioxaborolan-2-yl)benzonitrile (**2**).

Measurement of HPLC retention time. The HPLC retention time was measured with a Shimadzu LC-30A Nexera SR System equipped with a diode array detector and reversed-phase type ACQUITY CSH C-18 2.1 × 100 mm, 1.7 μm chromatographic columns.

Measurement of PL characteristics of thin films. The transient PL decay characteristics were measured at room temperature under a nitrogen atmosphere using a fluorescence spectrometer (PicoQuant, FluoTime 300) based on time-correlated single photon counting (PicoQuant, PicoHarp 300). A pulsed LED (PicoQuant, PLS 340) with an excitation wavelength of 340 nm and a single photon sensitive photomultiplier tube (PicoQuant, PMA-C) were used. The PL quantum yield (PLQY) were measured at room temperature under a nitrogen atmosphere using an absolute PLQY measurement system (Quantaurus-QY, Hamamatsu). The PL stability test and comparison between the as-deposited and 3-h UV-laser-exposed films was performed using a He-Cd laser (KIMMON KOHA, IK3202R-D) at 3.5 mW with an excitation wavelength of 325 nm. The films for the PL stability test were glass-encapsulated in a nitrogen-filled glove box after vacuum deposition. The angle-dependent PL was measured using a continuous wave laser (325 nm, Melles Griot). The incident angle of the excitation source was fixed at 45°. The angle dependent PL spectra of P-polarized light were detected using charge-coupled device (MAYA 2000, Ocean Optics).

Device fabrication and measurement. The organic layers were deposited on pre-cleaned ITO glass substrates using a thermal evaporation system with a vacuum pressure of $< 1.0 \cdot 10^{-6}$ torr. Layers of Liq (1 nm thick) and Al (100 nm thick) were deposited by thermal evaporation to form the cathode. The deposition rates of the organic and metal layers were about 0.1 and 0.5 nm s^{-1}, respectively, while that of the Liq layer was about 0.01 nm s^{-2}. The active device area of 4 mm^2 was defined by the overlapped area of the ITO and Al electrodes. The HOD structure was ITO/ p-doped BCFA (3 wt%, 10 nm) / BCFA (135 nm) /host(30 nm)/ BCFA (10 nm)/Al. The EOD structure was ITO/Ag/DBFPO:Liq(10 nm)/test material(30 nm)/DBFPO:Liq(30 nm)/Liq(1 nm)/Ag. The current, voltage, and luminance of the OLEDs were measured using a Keithley 2400 Source-Meter and Topcon SR-3ARspectroradiometer. Lifespan measurements of the OLEDs were performed under constant current.

Data availability. The data that support the findings of this study are available from the corresponding author upon reasonable request.

Declarations

Acknowledgements. The authors are grateful to Dr. Sangho Park for NMR measurements. The authors are gratefully acknowledge Analytical Engineering Group of Samsung Advanced Institute of Technology for access to their facility for NMR measurements.

Author contributions. S.-G.I., D.J., and E.S.K. contributed equally to this work. S.-G.I. conceived the study and performed the steady-state and transient PL measurements. S.-G.I., M.S. and S.N. fabricated the thin films and devices and performed device tests and analysis. D.J. established the polarity scale of the host materials to support the molecular design of the hosts. E.S.K., Sa.K and Y.S.C. synthesized and characterized the host materials. J.C. and Y.K. performed the HPLC retention time measurements. S.O.J. synthesized and characterized the TADF emitter. J.S.K. performed angle-dependent PL measurements. J.K. performed PL stability measurements. S.-G.I. analyzed the data and wrote the first version of the manuscript. All authors discussed the study and edited the manuscript. H.C. and Su.K. supervised the project.

Additional information. Supplementary information is available in the online version of the paper.

Competing financial interests. The authors declare no competing financial interests.

References

1. Méhes, G., Goushi, K., Postcavage, Jr., W. J.& Adachi, C.Influence of host matrix on thermally-activated delayed fluorescence: Effects on emission lifetime, photoluminescence quantum yield, and device performance. *Org. Electron.***15**, 2027–2037 (2014).
2. Holms, R. J., Forrest, S. R., Tung, Y.-J., Kwong, R. C. & Brown, J. J. Blue organic electrophosphorescence using exothermic host-guest energy transfer. *Appl. Phys. Lett.***82**, 2422–2024 (2003).
3. Tokito, S.,Iijima, T., Suzuri, Y., Kita, H., Tsuzuki, T. & Sato, T. Confinement of triplet energy on phosphorescent molecules for highly-efficient organic blue-light-emitting devices. *Appl. Phys. Lett.* **83**, 569–571 (2003).
4. Tanaka, I., Tabata, Y.&Tokito, S. Energy-transfer and light-emission mechanism of blue phosphorescent molecules in guest-host systems. *Chem. Phys. Lett.* **400**, 86–89 (2004).
5. dos Santos, P. L., Ward, J. S., Bryce, M. R.&Monkman, A. P. Using guest-host interactions to optimize the efficiency of TADF OLEDs. *J. Phys. Chem. Lett.* **7**, 3341–3346 (2016).
6. Dias, F. B., Penfold, T. J.&Monkman, A. P. Photophysics of thermally activated delayed fluorescence molecules. *Methods Appl. Fluoresc.* **5**, 012001 (2017).
7. Han C., Zhang, Z., Ding, D. & Xu, H. Diipole-dipole interaction management for efficient blue thermally activated delayed fluorescence diodes. *Chem* **4**, 2154–2167 (2018).
8. Zhang, Q., Li, J., Shizu, K., Huang, S., Hirata, S., Miyazaki, H. & Adachi, C. Design of efficient thermally activated delayed fluorescencematerials for pure blue organic light emitting diodes. *J. Am. Chem. Soc.* **134**, 14706 (2012).

9. Lee, S. Y., Yasuda, T., Yang, Y. S., Zhang, Q.& Adachi, C., Luminous butterflies: efficient excitonharvesting by benzophenone. *Angew. Chem.***126**, 6520–6524 (2014).
10. Kim, M., Jeon, S. K., Hwang, S.-H.& Lee, J. Y., Stable blue thermally activated delayed fluorescent organic light-emitting diodes with three timeslonger lifetime than phosphorescent organic light-emitting diodes. *Adv. Mater.***27**, 2515–2520 (2015).
11. Cho, Y. J., Jeon, S. K.& Lee, J. Y., Molecular engineering of high efficiency and long lifetime blue thermally activated delayed fluorescent emitters for vacuum and solution processed organic light-emitting diodes. *Adv. Optical Mater.* **4**, 688–693 (2016).
12. Lin, N.,Qiao, J., Duan, L., Li, H., Wang, L. &Qiu, Y.Achilles heels of phosphine oxide materials for OLEDs: Chemical stability and degradation mechanism of a bipolar phosphine oxide/carbazolehybrid host material. *J. Phys. Chem. C.* **116**, 19451–19457 (2012).
13. Lin, N., Qiao, J.,Duan. L., Wang, L.&Qiu, Y. Molecular understanding of the chemical stability of organic materials for OLEDs: A comparative study on sulfonyl, phosphine-oxide, and carbonyl-containing host materials. *J. Phys. Chem. C* **118**, 7569–7578 (2014).
14. Ihn, S.-G. *et al.* An alternative host material for long-lifespan blue organic light-emitting diodes using thermally activated delayed fluorescence. *Adv. Sci.***4**, 1600502 (2017).
15. Kim, M., Jeon, S. K., Hwang, S.-H. &Lee, J. Y. Stable blue thermally activated delayed fluorescent organic light-emitting diodes with three times longer lifetime than phosphorescent organic light-emitting diodes. *Adv. Mater.* **24**, 2515–2520 (2015)
16. Cho, Y. J., Jeon, S. K. & Lee, J. Y. Molecular engineering of high efficiency and long lifetime blue thermally activated delayed fluorescent emitters for vacuum and solution processed organic light-emitting diodes. *Adv. Opt. Mater.* **4**, 688–693 (2016)
17. Moldoveanu,S. C., David, V.*Essentials in Modern HPLC Separations* (Elsevier Inc., 2013).
18. Lee, K. H. *et al.* An excited state managing molecular design platform of blue thermally activated delayedfluorescence emitters by π-linker engineering. *J. Mater. Chem. C* **8**, 1736–1745 (2020).
19. Lippert, E., Lüder, W., Moll, F., Nägele, W., Boos, H., Prigge, H. & Seibold-Blankenstein, I. Umwandlung von Elektronenanregungsenergie. *Angew. Chem.* **73**, 695–706 (1961).
20. López-de-Luzuriaga, J. M., Manso, E., Monge, M., Olmos, N. E., Rodríguez-Castillo, M. & Sampedro, D. The effect of gold(I) coordination on the dual fluorescence of 4-(dimethylamino)pyridine. *Dalton Trans.***44**, 11029–11039 (2015).
21. Zeng, J.,Guo, J., Liu, H., Lam, J. W. Y., Zhao, Z., Chen, S. & Tang, B. Z. Aggregation-Induced Delayed Fluorescence Luminogens for Efficient Organic Light-Emitting Diodes. *Chem. Asian J.* **14**, 828–835 (2018).
22. Hong, S., Kim, J. W.& Lee, S. Lifetime enhanced phosphorescent organic light emitting diode using an electron scavenger layer. *Appl. Phys. Lett.* **107**, 041117 (2015).
23. Bulovic, V., Khalfin, V. B., Gu, G., Burrows, P. E., Garbuzov,D. Z.& Forrest, S. R. Weak microcavity effects in organic light-emitting devices. *Phys. Rev. B* **58**, 3730–3740 (1998).

24. Burrow, P. E.,Bulovic, V., Forrest, S. R., Sapochak, L. S., McCarty, D. M. & Thompson, M. E. Reliability and degradation of organic light emitting devices. *Appl. Phys. Lett.* **65**, 2922–2924 (1994).
25. Chatterjee, T. & Wong, K.-T., Perspective on Host Materials for Thermally Activated Delayed Fluorescence Organic Light Emitting Diodes. Adv. Opt. Mater. **7**, 1800565 (2019).
26. Yang, Z., Mao, Z., Xie, Z., Zhang, Y., Liu, S., Zhao, J., Xu, J., Chi, Z. &Aldred, M. P.Recent advances in organic thermally activated delayed fluorescence materials. *Soc. Rev.* **46**, 915–1016 (2017).
27. Park, J. H.,Seo, J. H., Lim, S. H., Ryu, G. Y., Shin, D. M. & Kim, Y. K. The effect of the molecular structure of organic material on the properties of solid-state fluorescence and electroluminescence. *J. Phys. Chem. Solids* **69**, 1314–1319 (2008).
28. Chen, C.-T.,Evolution of red organic light-emitting diodes: Materials and devices. *Chem. Mater.* **16**, 4389–4400(2004)
29. Burrows, P. E., Forrest, S. R., Sibley, S. P. & Thompson, M. E., Color-tunable organic light-emitting devices. *Appl. Phys. Lett.* **69**, 2959–2961(1996).
30. Materials Science Suite 2019-1 (Schrodinger, LLC, New York, NY, 2016).
31. Bochevarov, A.D., Harder, E., Hughes, T.F., Greenwood, J.R., Braden, D.A., Philipp, D.M., Rinaldo, D., Halls, M.D., Zhang, J., Friesner, R.A. Jaguar: A high-performance quantum chemistry software program with strengthsin life and materials sciences. *Int. J. Quantum Chem.***113**, 2110–2142 (2013).

Tables

Table 1. Calculated dipole moments of various hosts and photophysical properties of 1PCTrz-doped host films.

Host	μ_{GS}[a] [debye]	μ_{ES}[b] [debye]	μ_{PL}[c] [nm]	FWHM[d] [nm]	Quantum Yield [%]			τ_{PF}[e] [ns]	τ_{DF}[f] [µs]	k_{rISC}[g] [x10^5 s^{-1}]
					Delayed	Prompt	Total			
mCBP	0.80	0.79	457	80	23.8	39.9	63.7	11.3	18.8	0.85
mCBP-CN	3.40	3.31	458	79	10.9	52.0	62.9	10.9	10.3	1.12
H1	4.18	3.80	467	87	54.0	18.8	72.8	12.6	27.2	1.43
H2	6.84	11.73	470	87	37.9	37.0	74.9	11.9	15.0	1.35
H3	4.63	5.04	469	88	54.4	25.7	80.1	12.7	24.2	1.29
H4	7.64	7.73	466	88	47.3	32.0	79.3	11.7	20.7	1.19
DPEPO	8.05	11.06	471	88	46.5	32.5	79.0	14.0	13.3	1.82

[a] μ_{GS}: Ground-state dipole moment for the lowest energy conformer sampled from a conformational search and density functional theory (DFT) calculation at the B3LYP/6-31G(d) level. See Methods for details.

[b] μ_{ES}: Excited-state dipole moment obtained from time-dependent DFT calculation at the B3LYP/6-31G(d) level using the conformer corresponding to the lowest GS energy.

[c] λ_{PL}: Peak wavelength of the PL peak.

[d] FWHM: Full-width at half maximum.

[e] τ_{PF}: Prompt fluorescence lifetime.

[f] τ_{DF}: Delayed fluorescence lifetime.

[g] k_{rISC}: Rate constant of reverse intersystem crossing.

Table 2. Device performance of 1PCTrz-based OLEDs employing various hosts.

Host	Voltage[a]	Current efficiency[a]	Power efficiency[a]	EQE[b] (%)			LT50[c]
		(cd A^{-1})	(lm W^{-1})	Max	500 cd m^{-2}	1,000 cd m^{-2}	
	(V)						(h)
mCBP	5.60	12.85	7.22	10.0	8.4	7.5	3.3
mCBP-CN	4.58	11.86	8.14	9.1	7.5	7.2	36.2
H1	5.09	26.68	16.49	17.9	13.4	11.3	21.7
H2	5.60	20.52	11.51	13.6	9.5	8.4	122.4
H3	5.25	24.73	14.80	18.0	11.9	10.3	55.1
H4	5.47	26.32	15.13	16.3	12.1	10.6	86.9
DPEPO	7.62	20.41	8.42	21.1	9.9	7.5	0.6

[a] At 500 cd m^{-2}

[b] EQE: External quantum efficiency

[c] Time until the luminance decreased to 50% of the initial luminance of 500 cd m^{-2}.

Table 3. Out-coupling efficiency applying horizontal orientation of the transition dipole moment.

	$h/(h+\nu)$[a]	$\eta_{o.c.}$[b]
mCBP:1PCTrz	0.83	0.248
mCBP-CN:1PCTrz	0.88	0.263
H1:1PCTrz	0.87	0.260
H2:1PCTrz	0.89	0.266
H3:1PCTrz	0.79	0.236
H3:1PCTrz	0.88	0.263
DPEPO:1PCTrz	0.87	0.260

[a] Horizontal orientation of transition dipole moment.

[b]Out-coupling efficiency applying $h/(h+\nu)$. In case of the perfect isotropic orientation, $\eta_{o.c.} = 0.2$.

Figures

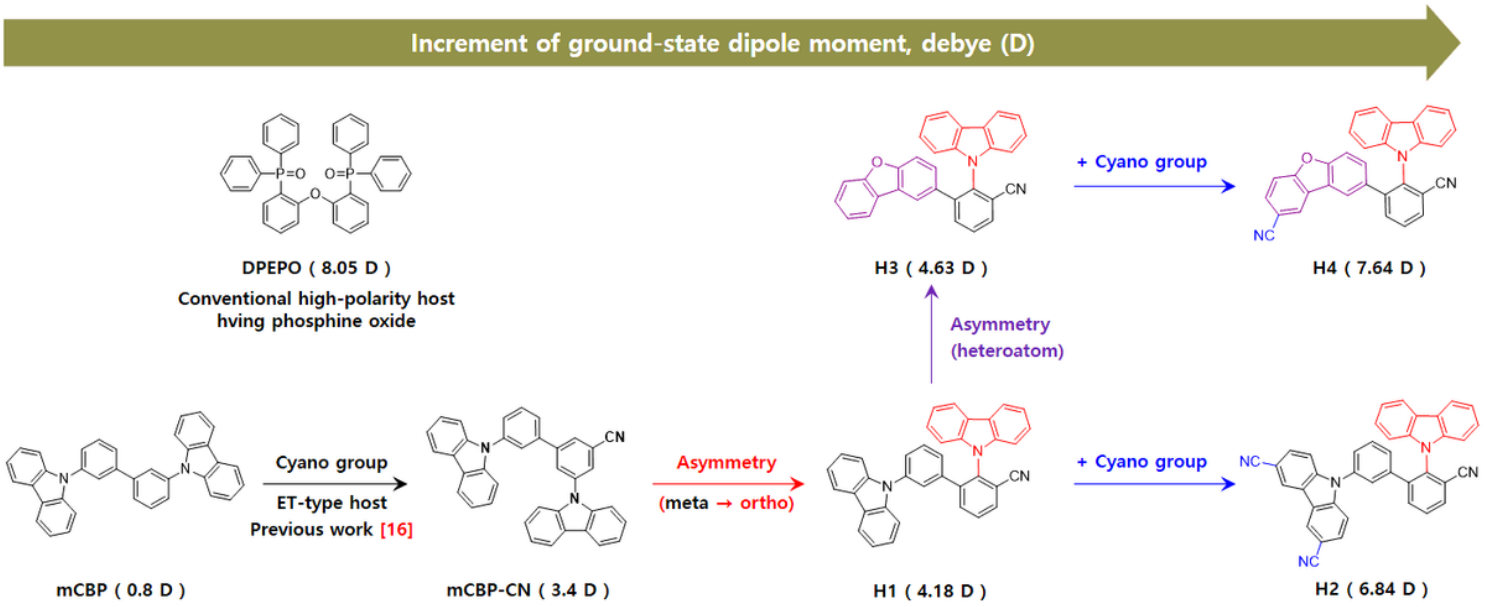

Figure 1

Design strategies for high-polarity host materials and their chemical structures. Strategies for increasing the polarity of host materials by means of increasing structural asymmetry and their examples (H1–H4, derivatives of mCBP-CN). The values in the brackets are the calculated ground-state dipole moments, μGS, in debye (D).

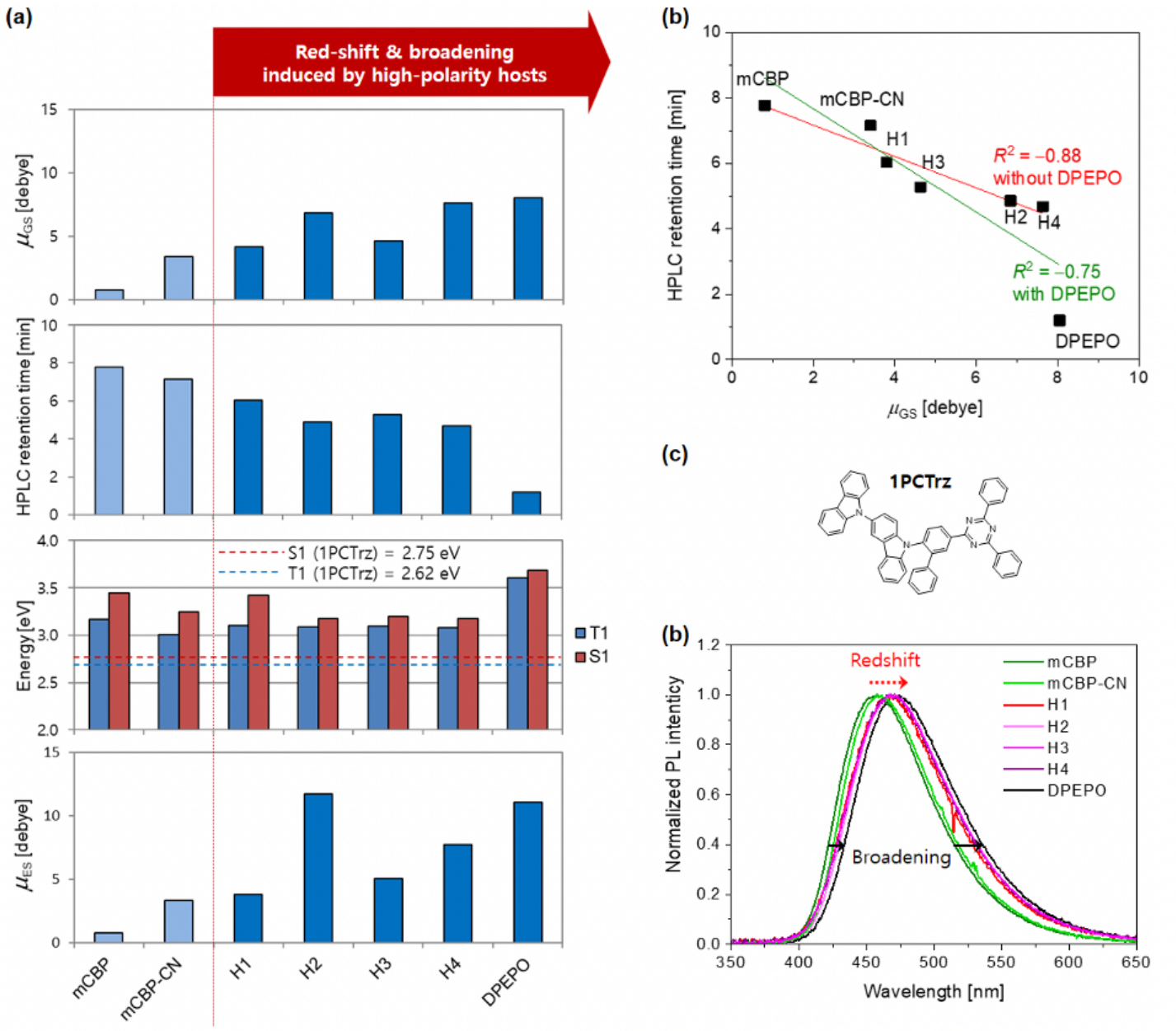

Figure 2

Increased host polarity correlates with reduced HPLC retention time and redshifted and broadened photoluminescence (PL) spectra. a. Calculated values of ground-state dipole moments, μGS (first panel); HPLC retention time (second panel); T1 and S1 energies (third panel) and calculated values of excited-state dipole moments, μES (fourth panel) of the hosts. b. Correlation between ground-state dipole moment and HPLC retention time. c. Chemical structure of TADF emitter, 1PCTrz. d. Photoluminescence spectra of 1PCTrz in the various host materials. Compared to the emission peaks of 1PCTrz in mCBP and mCBP-CN, those in H1–H4 and DPEPO are redshifted (red dotted arrow) and broadened (black solid arrows). μGS, μES, T1, and S1 are represented as the values corresponding to the minimum energy structure for each host (See also Figure S1 and Table 1.).

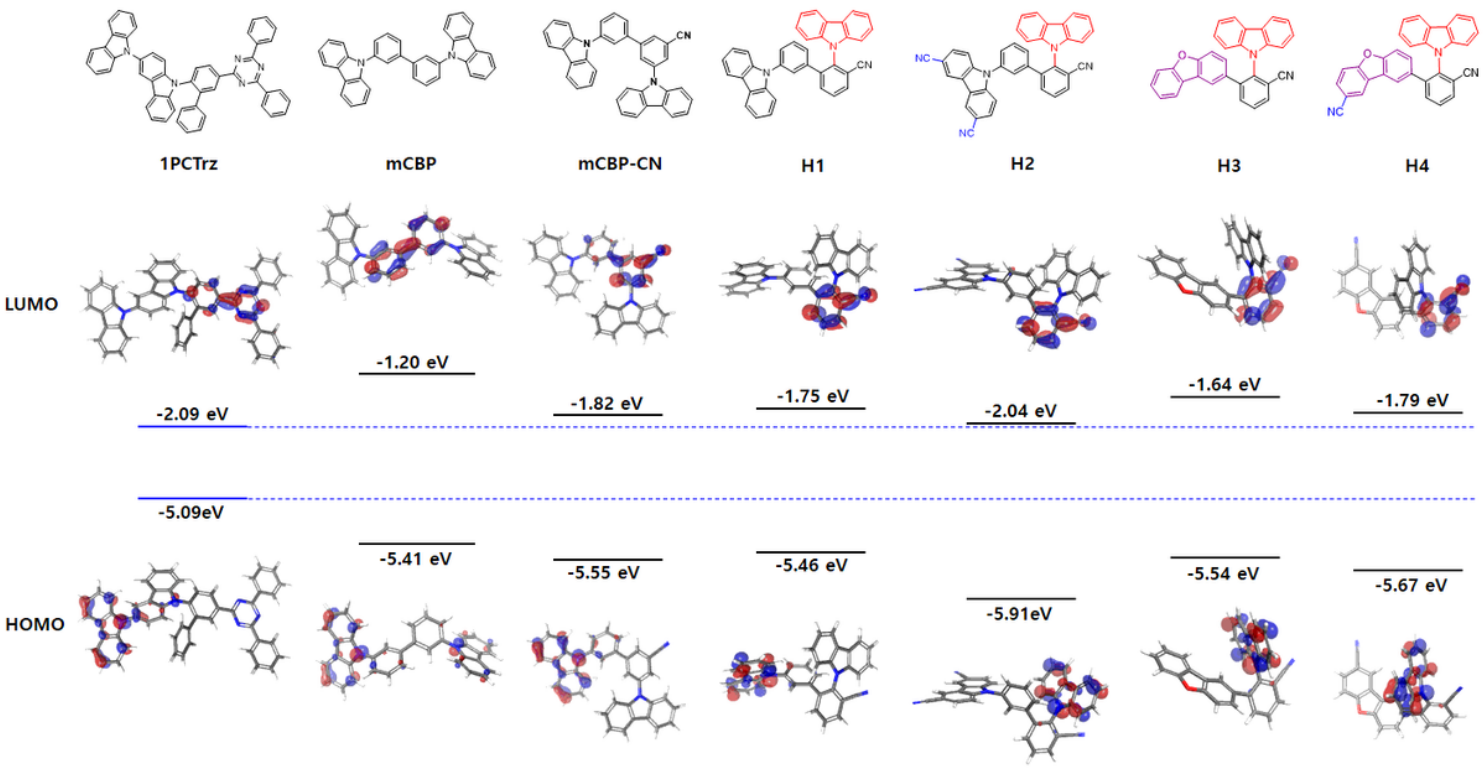

Figure 3

Ground-state characteristics of 1PCTrz and various hosts. Contours of HOMOs and LUMOs and their energy levels. The HOMO energy levels of the hosts are all much lower than that of 1PCTrz, while the LUMO energy levels of the hosts are slightly shallower than that of 1PCTrz, except for that of mCBP, which is considerably lower.

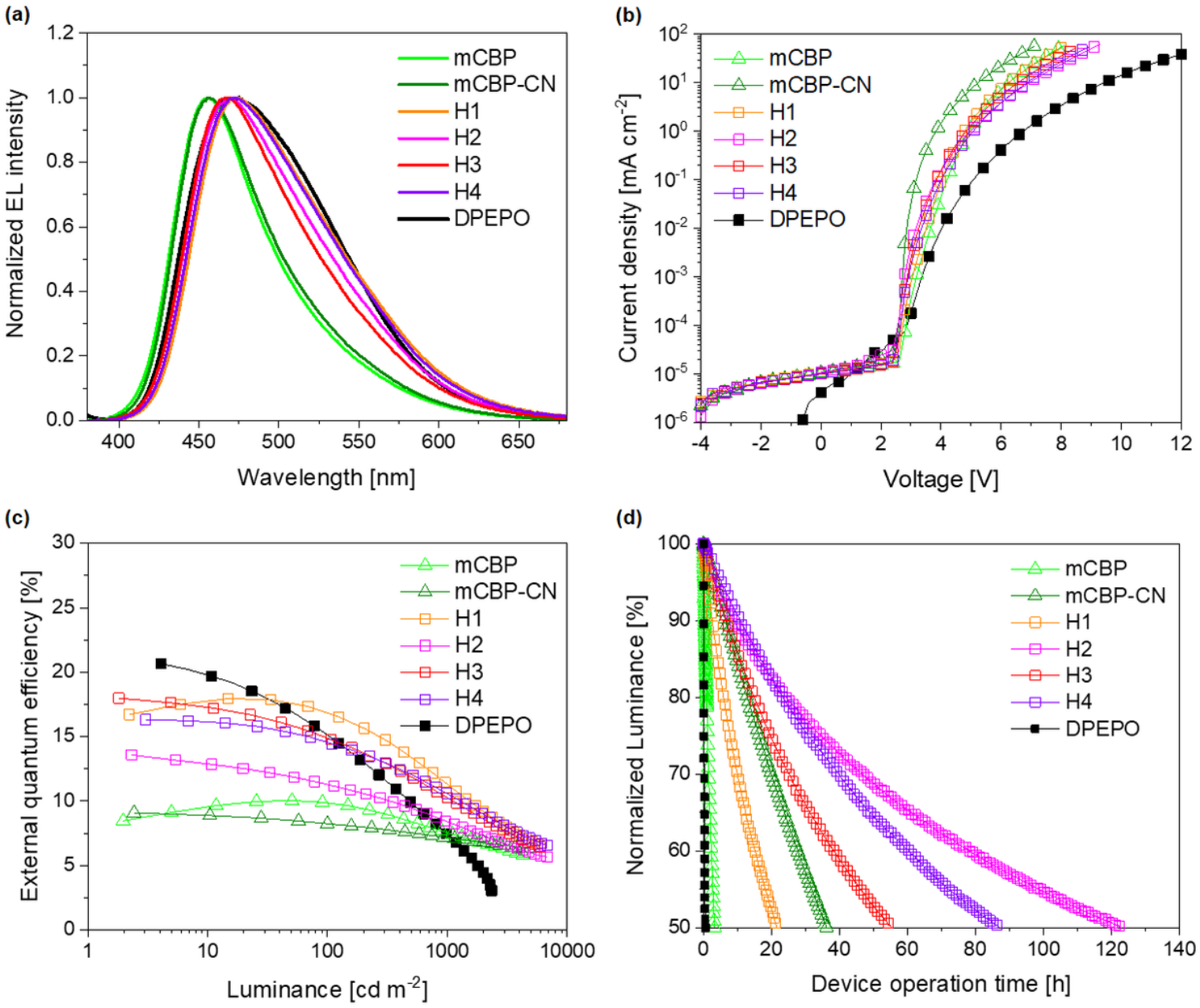

Figure 4

Characteristics of OLEDs. a. Electroluminescence spectra of the OLEDs at 500 cd m-2. b. Current density–voltage characteristics for the OLEDs. c. EQE of the OLEDs as a function of luminance. d. Normalized luminance of the OLEDs as a function of operation time at a constant current density. The initial luminance was 500 cd m-2.

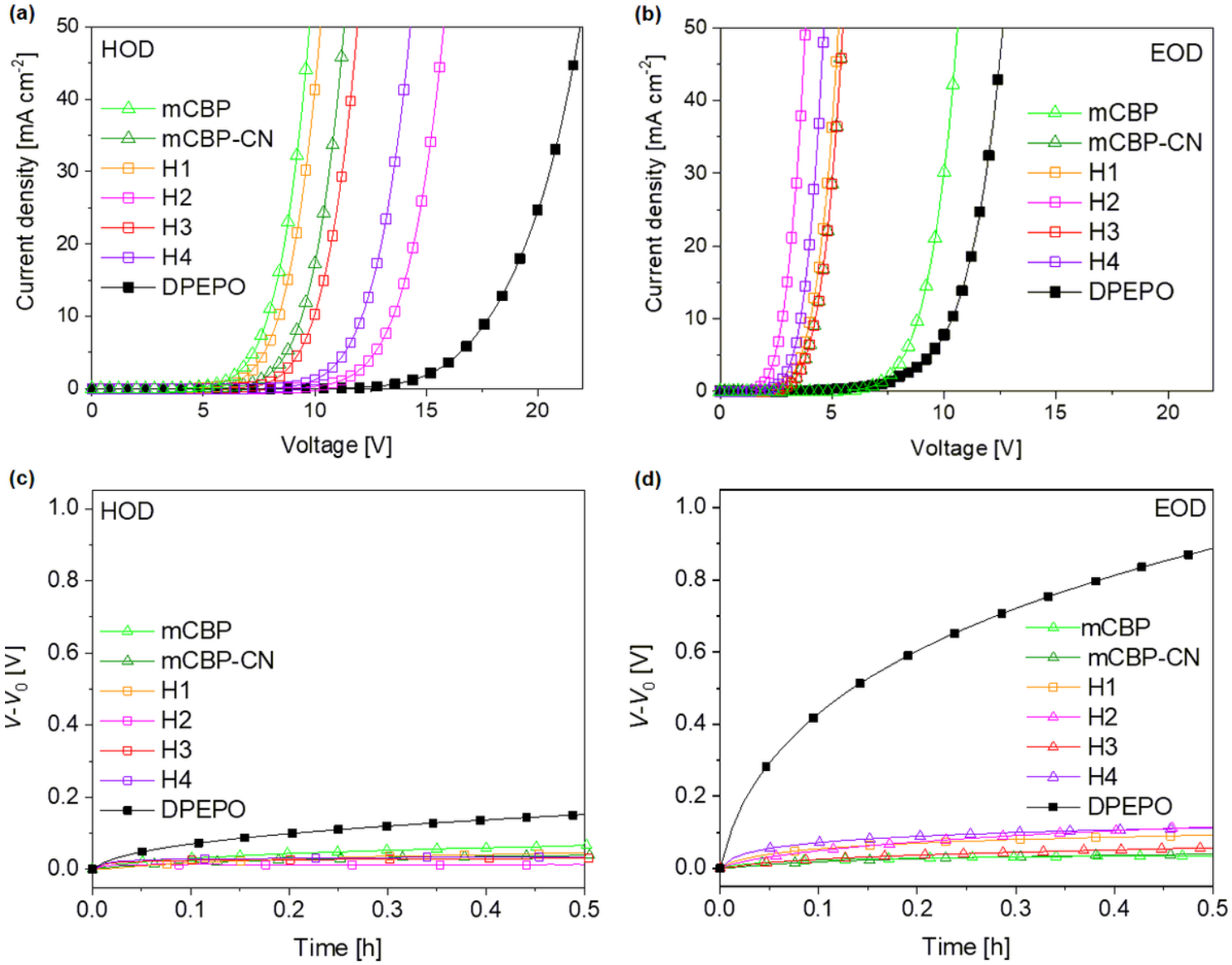

Figure 5

Characteristics of hole-only devices (HODs), and electron-only devices (EODs). a. and b. Current density–voltage curves of HODs and EODs, respectively, for various host films. c. and d. Changes of the driving voltages of HODs and EODs, respectively, for various host films as a function of operation time with constant driving current. V0 is the initial voltage.

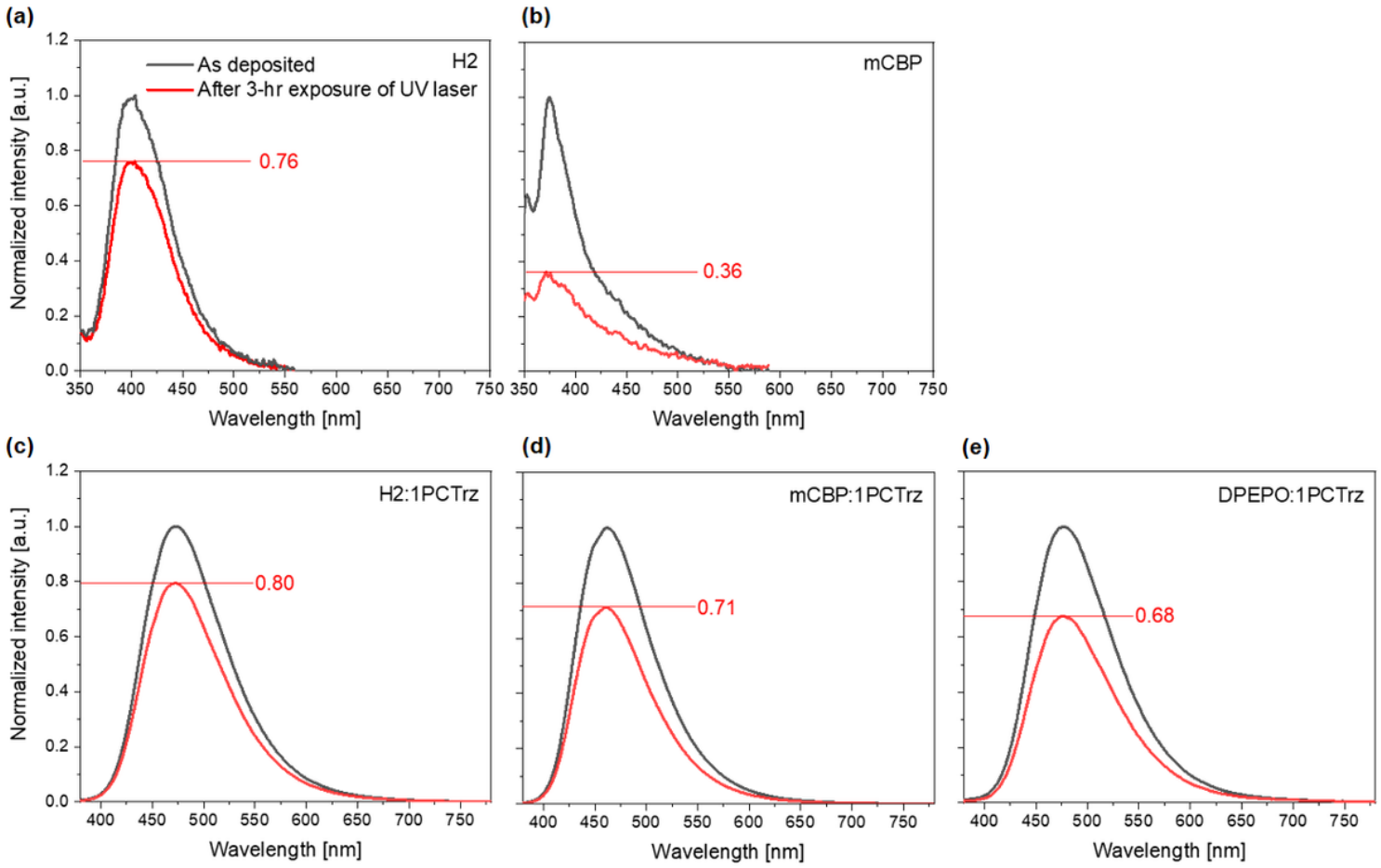

Figure 6

PL stability of various host films. PL spectra of the a. H2, b. mCBP, c. H2:1PCTrz, d. mCBP:1PCTrz and e. DPEPO:1PCTrz films. The black PL spectra were achieved from the as-deposited films while the red PL spectra were achieved from the very films after 3-hr exposure to UV laser. The composition ratios of the co-deposited films are all 85:15 by volume. See also Supplementary Figure 2.

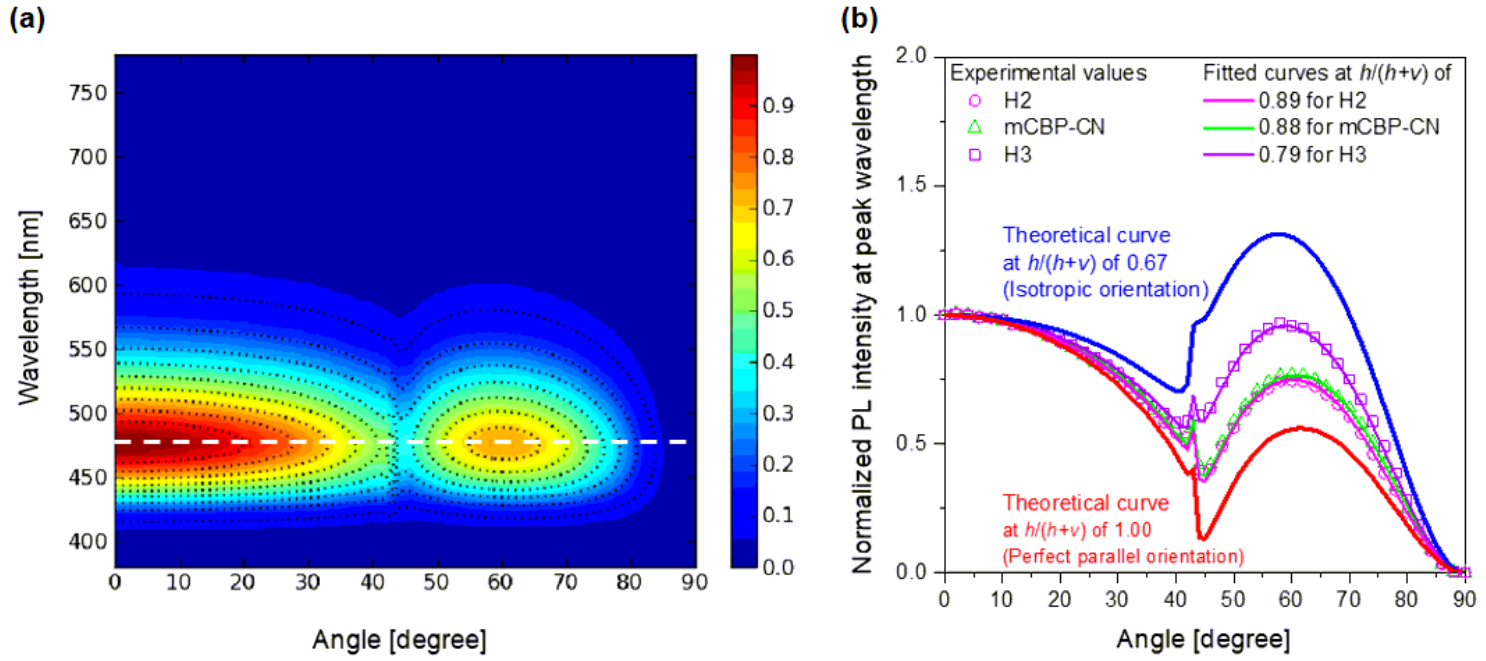

Figure 7

Analysis of the horizontal orientations of the transition dipole moments (h/(h+v)). a. Angle-dependent PL spectrum of p-polarized light from a 50-nm-thick H2:1PCTrz (85:15 by volume) film. b. Angle-dependent PL intensities at peak wavelengths. The magenta open squares represent the PL intensity from the H2:1PCTrz film, which are equivalent to the white dashed line in a. The green triangles and purple squares represent the PL intensities from mCBP:1PCTrz (85:15) and a H3:1PCTrz (85:15) films, respectively. Inspection of the solid curves for the films of the three 15% 1PCTrz-doped hosts (H2, mCBP-CN and H3) reveal horizontal orientations of the transition dipole moment (h/(h+v)) of 0.89, 0.88 and 0.79, respectively. The blue and red lines correspond totheoretical curves constructed with h/(h+v) values of 0.67 (isotropic orientation) and 1.0 (perfect parallel orientation), respectively. See also Supplementary Figure 3.

Supplementary Files

This is a list of supplementary files associated with this preprint. Click to download.

- SupplementaryInformationlhn.docx